A novel system applying artificial intelligence in the identification of air leak sites

Check for updates

Yuka Kadomatsu, MD, PhD,[a] Megumi Nakao, PhD,[b] Harushi Ueno, MD,[a] Shota Nakamura, MD, PhD,[a] and Toyofumi Fengshi Chen-Yoshikawa, MD, PhD[a]

ABSTRACT

Objective: Prolonged air leak is the most common complication of thoracic surgery. Intraoperative leak site detection is the first step in decreasing the risk of leak-related postoperative complications.

Methods: We retrospectively reviewed the surgical videos of patients who underwent lung resection at our institution. In the training phase, deep learning-based air leak detection software was developed using leak-positive endoscopic images. In the testing phase, a different data set was used to evaluate our proposed application for each predicted box.

Results: A total of 110 originally captured and labeled images obtained from 70 surgeries were preprocessed for the training data set. The testing data set contained 64 leak-positive and 45 leak-negative sites. The testing data set was obtained from 93 operations, including 58 patients in whom an air leak was present and 35 patients in whom an air leak was absent. In the testing phase, our software detected leak sites with a sensitivity and specificity of 81.3% and 68.9%, respectively.

Conclusions: We have successfully developed a deep learning-based leak site detection application, which can be used in deflated lungs. Although the current version is still a prototype with a limited training data set, it is a novel concept of leak detection based entirely on visual information. (JTCVS Techniques 2022;15:181-91)
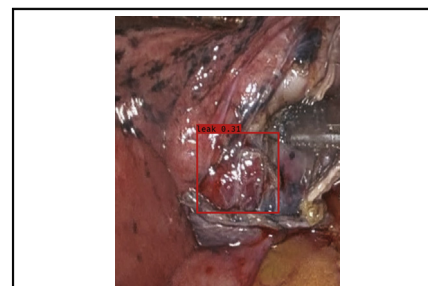
Output image of leak site detection software using a deep learning algorithm.

CENTRAL MESSAGE

We developed novel leak site detection software using a deep learning algorithm on the basis of only intraoperative visual information.

PERSPECTIVE

We developed novel deep learning-based air leak detection software to automatically estimate potential leak sites from intraoperative images. We retrospectively assessed the usefulness of this software. Although the current version is in a preliminary phase and works with a limited training data set, we still obtained good sensitivity and specificity.

▶ Video clip is available online.

https://doi.org/10.1016/j.xjtc.2022.06.011

Prolonged air leak is the most common complication of pulmonary resection and one of the factors that prolong hospital stay.[1] To find the leak point, a leak test is performed by immersing the thoracic cavity in water and observing air leakage from the lung surface before closing the wound. However, in these days of minimally invasive surgeries, such as video-assisted thoracoscopic surgery and robot-assisted thoracoscopic surgery (RATS), the problems of poor visibility due to the inflated lung itself and damage of nonphysiologic positive pressure ventilation to the lung parenchyma during the conventional leak test have been recognized. Detecting a spot that requires extra treatment to prevent or treat air leaks could reduce medical costs, patients' burden of prolonged air leak-related complications, and hospital stay.

Among recent advances in computer vision studies, J. Redmon developed a real-time object detection framework using deep learning methods.[2] "Object detection" is a computer algorithm for locating and recognizing specific objects in images or videos. This framework has been previously applied to detect bone fractures and tumors in radiography.[3,4] However, it has not been applied to detect specific anatomical structures or organs during surgery. The algorithm is an open-source system that can show the existence and range of an object to be detected from an unknown image by examining the visual information. The processing speed is high, indicating that the method can be used as a real-time detection method for static images as well as for videos.[5]

The procedures in RATS, which have no tactile sense, are primarily performed on the basis of the fine visual image. Moreover, with the development of vision systems, such as 4K and 3D endoscopic cameras, more detailed images are helping surgeons perform more complex procedures in recent minimally invasive surgery.[6] The importance of visual information in thoracic surgery is gradually increasing.

A leak site is a lung area where the lung surface is missing or damaged. We attempted to develop an algorithm to automatically detect a "potential leak site" that has the objective appearance of the surface of the lung that is associated with an elevated risk of air leak. In this study we aimed to evaluate the clinical applicability of the prototype application.
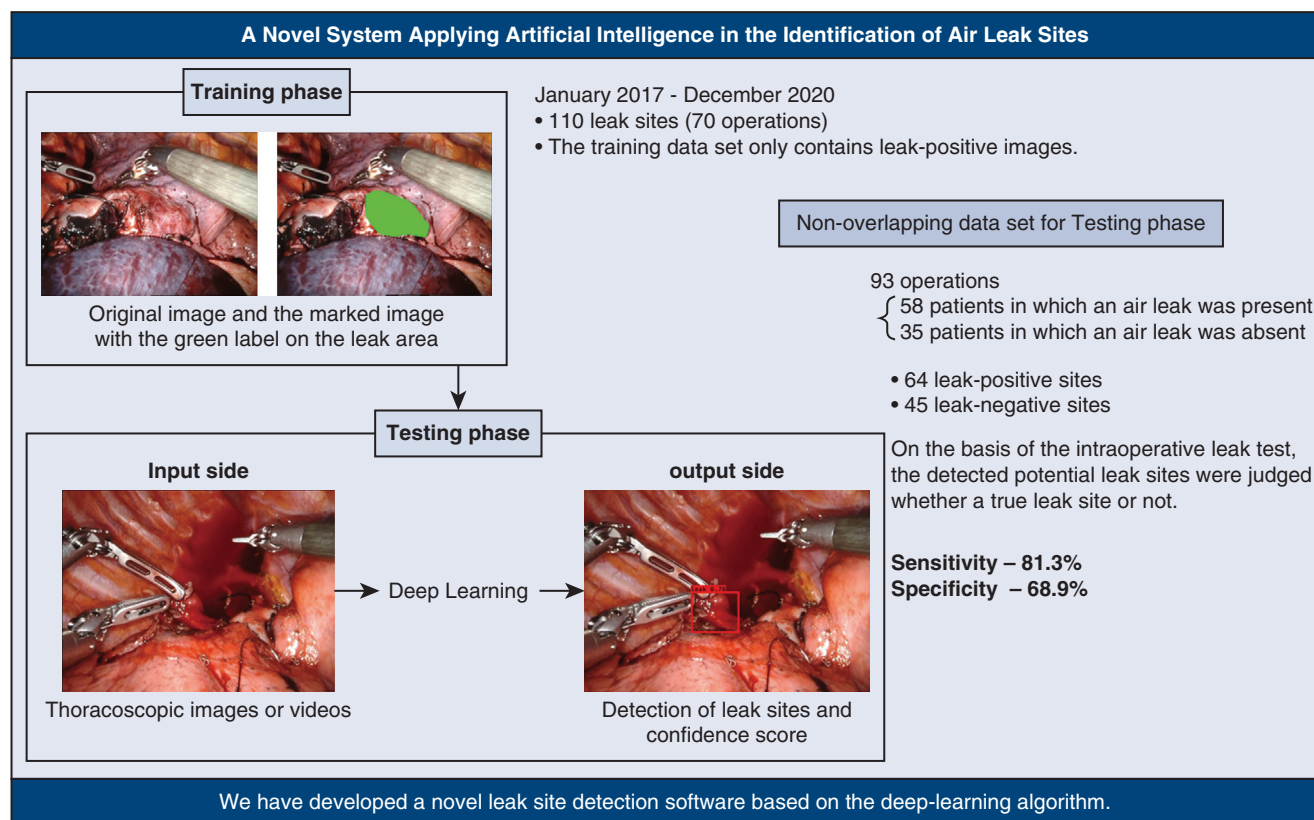
METHODS
Development of Our Novel Application

This study comprised 2 major phases: training phase and testing phase (Figure 1). Different data sets without overlapping data were used during the testing and training phases. The testing data set included 109 detected sites containing 64 leak-positive sites and 45 leak-negative sites. The testing data set was obtained from 93 operations, including 58 patients in whom an air leak was present and 35 patients in whom an air leak was absent. During the training phase, for each leak site, we prepared the original image and labeled image with the leak area marked in color (Figure 2). Our proposed software obtains an endoscopic image as the input and outputs leak area if a leak site is detected in the image. The input endoscopic image was divided into $S \times S$ nonoverlapped grid cells, and each cell detects the potential leak site belonging to the grid cell, as applied in Redmon.[2] The output image is presented in Figure 1. The red rectangular box (ie, predicted box) shows the algorithm-based predicted leak area by our developed software. The confidence score is the representative value of the probability that a leak site exists in the predicted box. This confidence score is a value that can range from 0 to 1, where a score of 0 represents a grid cell that does not contain any "potential leak site: lung parenchyma that has the objective appearance associated with an elevated risk of an air leak" and 1 represents 100% confidence that a "leak site" is present in the predicted grid cell.
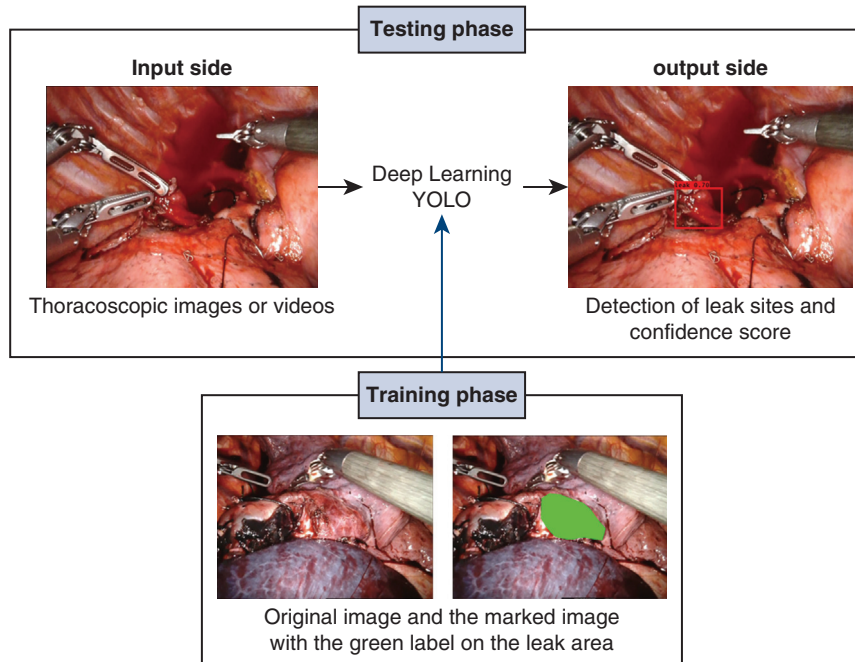
FIGURE 1. Schematic diagram of this study, consisting of training and testing phases. The 110 pairs of the original and leak site marked images were used in the training data set, whereas another set of thoracoscopic images and videos were used to evaluate the performance of the developed software. *YOLO*, You Only Look Once.

A Novel System Applying Artificial Intelligence in the Identification of Air Leak Sites

Training phase

Original image and the marked image
with the green label on the leak area

January 2017 - December 2020
• 110 leak sites (70 operations)
• The training data set only contains leak-positive images.

Non-overlapping data set for Testing phase

93 operations
{ 58 patients in which an air leak was present
35 patients in which an air leak was absent

• 64 leak-positive sites
• 45 leak-negative sites

On the basis of the intraoperative leak test, the detected potential leak sites were judged whether a true leak site or not.

Sensitivity – 81.3%
Specificity – 68.9%

Testing phase

Input side   **output side**

Thoracoscopic images or videos → Deep Learning → Detection of leak sites and confidence score

We have developed a novel leak site detection software based on the deep-learning algorithm.

FIGURE 2. This novel software detects the presence or absence of potential leak sites in intraoperative static images or videos via endoscopic camera.

Training and Testing Data Set

We retrospectively reviewed the surgical videos of patients who underwent pulmonary resection at our institution. In collecting leak-positive images, we defined the inclusion criteria according to the following 3 conditions: cases in which the presence of an intraoperative leak using the conventional leak test was described in the surgical record; cases in which surgical videos were preserved and intraoperative leak tests were recorded; and cases in which the leak area can be visually confirmed. During the pilot development phase, training data sets were often collected in hundreds,[2,7] so we aimed to collect data from 100 leak sites for the prototype application. One surgeon (Y.K.) identified the true leak site from the conventional air leak test in the surgical videos. One frame containing the leak site in the video was screen-captured per single leak site, and the image with the leak area was marked with color (training phase; Figure 1). We collected 110 images of leak sites from 70 surgeries. These 110 labeled and originally captured images were randomly translated, clipped, and scaled. This preprocess creates various patterns of local images and improves stability of learning. Hence, we used clipped images with 416×416 pixels as the training data set, 32 for each training batch and 300 for the total number of training epochs to train the application.

In the testing phase, we evaluated our application using another data set. We prepared cases with a confirmed air leak site and cases without air leak using the traditional leak test. The leak-positive test data consisted of images selected from consecutive cases between January 2021 and September 2021, on the basis of the same inclusion criteria in the training data set. For the leak-positive cases, the captured image was trimmed in the following conditions: there was a large amount of saline remaining in the thoracic cavity, the text was displayed, and the leak site was biased toward the edges

of the screen. In collecting leak-negative images, we defined the inclusion criteria as the following 2 conditions: cases in which the intrathoracic saline had been sufficiently removed after a conventional leak test, and cases in which the hilar and residual lung parenchymas were recorded for >5 seconds in the surgical video. Considering these criteria, leak-negative surgeries were randomly selected. The target number of images was set at approximately half of the cases of leak-positive images between May 2019 and September 2021.

Only 1 frame from the surgical video was screen-captured per each leak site, and we did not recapture another frame of the same leak site after evaluation by the application. This study was conducted on a PC Intel Core i7-10700 with 32 GB RAM, clock speed or frequency of CPU at 2.90 GHz, and GPU of NVIDIA GeForce RTX 2070 SUPER.

Performance Evaluation Measures

In our developed software, multiple predicted boxes may be displayed in a single output. Therefore, we categorized each predicted box into 4 categories: true positive (TP), false positive (FP), true negative (TN), and false negative (FN). We objectively evaluated the performance in terms of sensitivity and specificity (Figure 3). The area under the receiver operating curve and Youden index were calculated to assess the optimal cutoff value for the confidence score. Specifically, this method determines the optimal cutoff point as the tangent-based point that is closest to the point of the (0, 1) coordinates in Figure 4. This model was also evaluated using precision and recall scores to compare its usefulness with that of previously reported models that use deep learning algorithms. The precision score (%) was calculated as $TP/(TP + FP) \times 100$, which is the same index as the so-called positive predictive value. The recall score (%) was calculated as $TP/(TP + FN) \times 100$.[8]
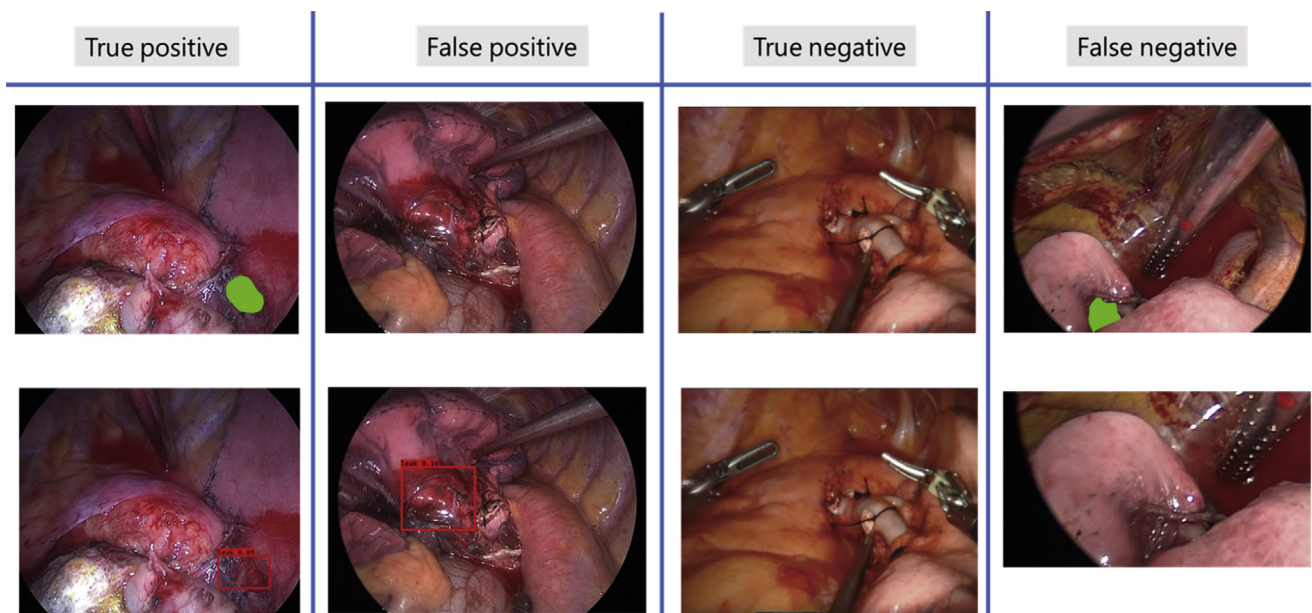
FIGURE 3. Sample image of each category (true positive, false positive, true negative, and false-negative).

The study protocol was approved by the institutional review board of Nagoya University School of Medicine (2015-0458, March 8, 2016). The requirement for informed consent was waived because of the retrospective study design.

RESULTS

Figure 5 presents 2 cases of our application's ability to detect the leak site on the intraoperative endoscopic images, with Figure 5, *A* and *D* showing the actual leak site. To compare the actual leak site and predicted site in the testing phase, the leak site was colored in green in advance when the testing data set was constructed, as shown in Figure 5, *B* and *E*. Figure 5, *C* and *F* show the leak sites detected by our developed model. Of the 238 surgeries with lung resection performed in the testing phase, 90 (37.8%) had leaks in the conventional leak test. We obtained 64 leak-positive sites and 11 leak-negative sites from 58 (64%) of the surgeries. We obtained 35 leak-negative sites from 35 of 397 (8.8%) leak-negative surgeries. Clinical information of the testing data set is shown in Table E1. Overall, the testing data set contained 64 leak-positive sites and 45 leak-negative sites. As noted in the Methods section, each predicted box has a confidence score representing the probability that the leak site is in the predicted box. When the cutoff value of the confidence score was set at 0, the number of TP, FP, TN, and FN boxes were 52, 14, 31, and 12, respectively. As a result, the sensitivity and specificity were 81.3% and 68.9%, respectively. The precision was 78.7%, and the recall was 81.3%. The receiver operating characteristic curve is presented in Figure 4, and the area under the receiver operating characteristic curve was 0.689. There was an optimal cutoff value of 0.09, with a sensitivity of 62.5% and specificity of 69.2%.

Our developed software simultaneously predicts multiple bounding boxes, and we can process streaming video almost in real time. Although it is still the preliminary stage, we verified the results with a video clip of a scene after a traditional leak test, and our software detected the same as a still image (Video 1).

DISCUSSION

In this study, we developed deep learning-based software that detects the presence or absence of leaks in the locations of potential air leak sites on endoscopic surgical images. If an air leak is known to be present at the time of postresection visual inspection, additional therapy could be applied to reduce the severity or duration of that air leak. Prolonged air leak after lung resection is the most common complication and is related to long hospital stay and high cost.[1,9] Prolonged air leak also leads to other complications, such as empyema and wound infection. There is no definitive definition of prolonged air leak, but several studies defined it as a condition lasting more than 5 to 10 days.[9] Moreover, the intensity of intraoperative air leaks has been associated with the duration of postoperative leaks.[10] Therefore, detection of the air leak site is the first step in reducing air leak-related postoperative complications, shortening hospital stays, and reducing medical costs.[10]

Recently, an automatic diagnostic system on the basis of deep learning algorithms has been proposed, and some clinical applications have been initiated.[11] However, this trend has been limited to pathology and radiology, where human
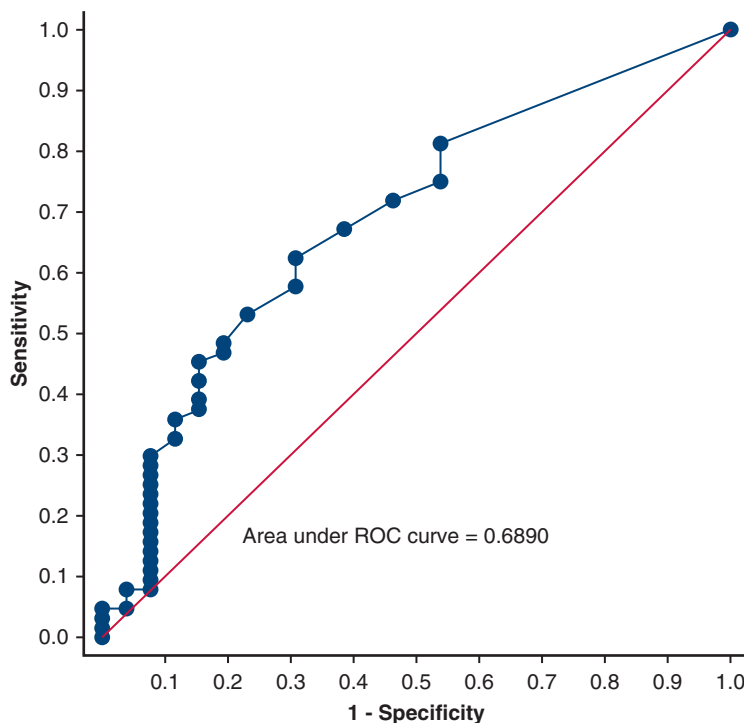
FIGURE 4. Receiver operating characteristic (*ROC*) curve of the confidence score to predict the leak site. The optimal cutoff value was 0.09 for the confidence score of each bounding box.

experts have originally made visual decisions, and it is a substitute for that process.[2,8] In contrast, the leak site detection procedure has not traditionally used visual detection. The conventional submersion test is conducted by inflating the lung within the saline-filled pleural cavity.[12] Surgeons do not find the leak site by direct visual inspection but by following the bubbles that leak from the damaged lung surface. Recently, with the increased application of minimally invasive surgeries, the inflated lung parenchyma itself might block the surgeon's view and prevent a high-quality leak test.[10,13] Although there have been attempts to develop new leak test methods, a new technique that does not require inflation has not been introduced so far.

The precision and recall of the software were 78.7% and 81.3%, respectively. Because there is no previous deep learning-based application in the field of leak testing, it is difficult to compare the performance of our proposed application. In the previously reported outcomes in the prototype application in radiology and pathology, precision and recall are approximately 87% to 93% and 65% to 88%, respectively.[4,8] Compared with previous studies, the precision score of the current model is slightly lower. This indicates that it is detecting regions other than the leak sites, creating FP cases. For example, our software detected areas, such as the mediastinal fat and surgical instruments (Figure E1). In contrast, FN cases were also apparent, in which the appearance of the leak site was similar to the color of the background lung (Figure E2). These FP and undetected cases

are expected to decrease in the future as the amount of training data increase.

This software has 3 strengths. First, it is on the basis of a deep learning algorithm, which is expected to provide a smooth transition from images to videos. Second, this software would not require lung inflation, which allows us to have sufficient working space, even in minimally invasive surgery. Last, we found the deep learning-based algorithm to be good at detecting small, damaged areas that are sometimes difficult to detect with the human eye (Figure 5, *D-F*).

This study has several limitations. First, the captured surgical endoscopic images were retrospectively extracted from recorded videos. In future prospective clinical trials, the method of how we screened the lung surface would be of importance. Without appropriate manipulation, there might be areas of leakage that might not be visible. This would influence the ability to detect "unsuspected" areas of leakage. Second, in leak-negative cases, when the conventional leak test did not reveal a leak, the residual lung surface was not observed. Therefore, it is unclear how this application would be effective when manipulating the lung surface without knowing whether there is a leak. Third, in cases featuring leakage from the automatic suturing line, surgeons sometimes cannot find the leak sites even after careful visual inspection. In this study, we excluded cases in which the leak site was not visible in either the training data set or validation data set, so detection of leakage of this type is not expected at present. If the resolution of
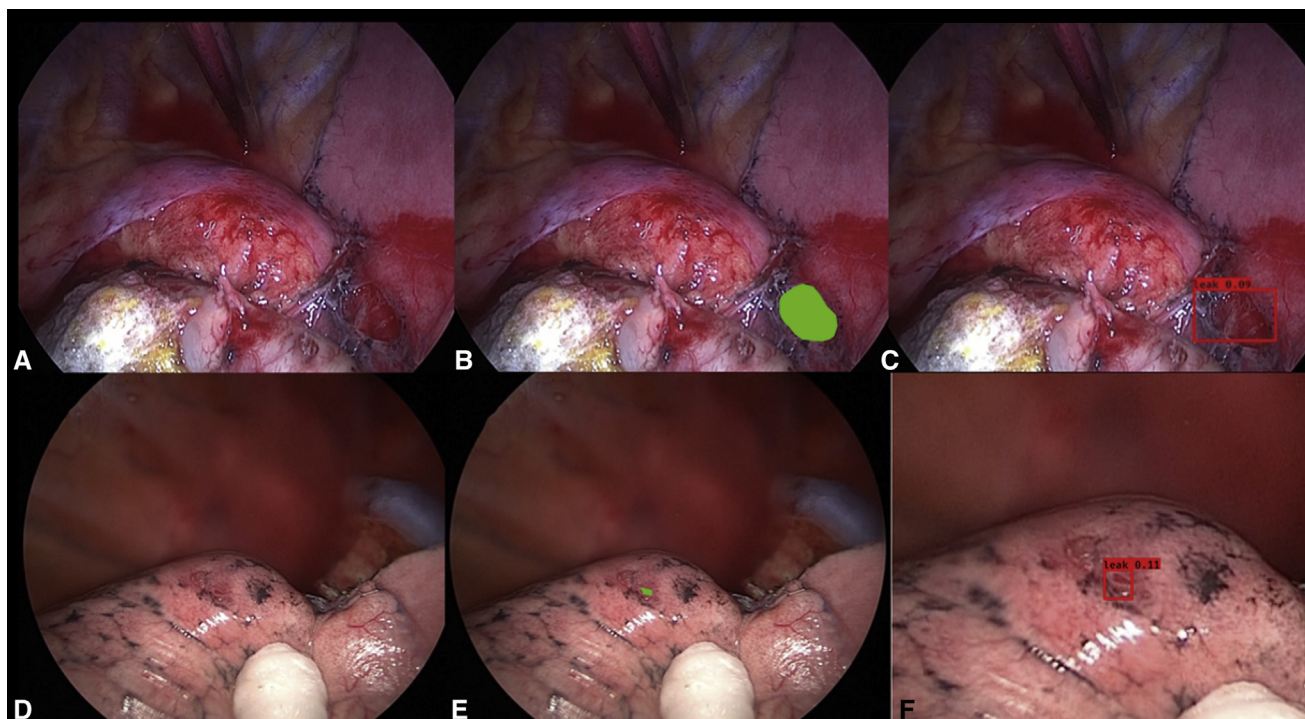
FIGURE 5. Sample cases of leak site detection. A and D, The original captured image. B and E, The actual leak site detected using the traditional leak test. C and F, The output images from the application. The lower case had a large amount of saline remaining in the cavity, and the part of the background was trimmed as shown in (F) before running the application.

endoscopic cameras is improved so that they can detect small deficits more effectively than the human eye, it might be possible to train the detection of these types of leaks. Fourth, the current version is still in a preliminary phase and works with extremely limited training data. When the predicted box is more precise, this application would be more useful. In the future, we would like to conduct a multi-center prospective study to upgrade this application, making it more useful and contributing to the reduction in prolonged and unexpected postoperative lung leaks after lung resection. Finally, this study was conducted on the

basis of the latest artificial intelligence theory, and we acknowledge a certain difficulty to understand for the general clinicians. The 2 publications that introduced machine learning related to the medical field might help this discrepancy.[14,15]

CONCLUSIONS

We have developed a pulmonary air leak site detection application on the basis of still images of deflated lung tissue obtained from a robotic or thoracoscopic camera immediately after pulmonary resection. The concept of our application is on the basis of visual information only, which could change the concept of conventional leak tests and allow appropriate intervention to reduce or mitigate air leaks.

Conflict of Interest Statement

The authors have obtained a patent for this leak detection technique. At the time of writing this report, this technology had not been commercialized and no financial ties had yet been planned. The authors reported no conflicts of interest.

The *Journal* policy requires editors and reviewers to disclose conflicts of interest and to decline handling or reviewing manuscripts for which they may have a conflict of interest. The editors and reviewers of this article have no conflicts of interest.
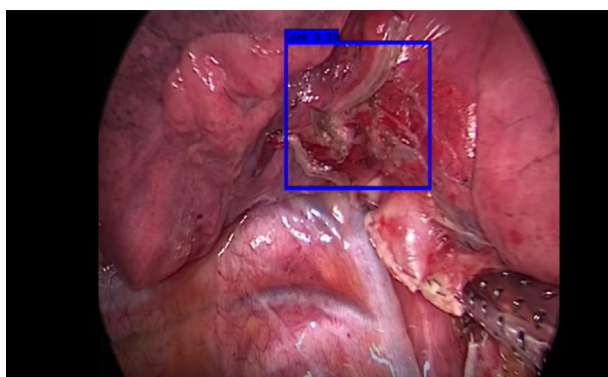
VIDEO 1. Application of our developed application to endoscopic surgical videos. Video available at: https://www.jtcvs.org/article/S2666-2507(22)00365-0/fulltext.

References

1. Hoeijmakers F, Hartemink KJ, Verhagen AF, Steup WH, Marra E, Röell WFB, et al. Variation in incidence, prevention and treatment of persistent air leak after lung cancer surgery. *Eur J Cardiothorac Surg*. 2021;61:110-7. https://doi.org/10.1093/ejcts/ezab376
2. Redmon J, Farhadi A. YOLO9000: better, faster, stronger. Paper presented at: IEEE Conference on Computer Vision and Pattern Recognition; July 21-26, 2017; Honolulu.
3. Al-Masni MA, Al-Antari MA, Park JM, Gi G, Kim TY, Rivera P, et al. Simultaneous detection and classification of breast masses in digital mammograms via a deep learning YOLO-based CAD system. *Comput Methods Programs Biomed*. 2018;157:85-94. https://doi.org/10.1016/j.cmpb.2018.01.017
4. Son DM, Yoon YA, Kwon HJ, An CH, Lee SH. Automatic detection of mandibular fractures in panoramic radiographs using deep learning. *Diagnostics (Basel)*. 2021;11:933. https://doi.org/10.3390/diagnostics11060933
5. Wang Z, Walsh K, Koirala A. Mango fruit load estimation using a video based MangoYOLO-Kalman Filter-Hungarian algorithm method. *Sensors (Basel)*. 2019;19:2742. https://doi.org/10.3390/s19122742
6. Abdelrahman M, Belramman A, Salem R, Patel B. Acquiring basic and advanced laparoscopic skills in novices using two-dimensional (2D), three-dimensional (3D) and ultra-high definition (4K) vision systems: a randomized control study. *Int J Surg*. 2018;53:333-8. https://doi.org/10.1016/j.ijsu.2018.03.080
7. Zheng Y, Zhang R, Yu R, Jiang Y, Mak TWC, Wong SH, et al. Localisation of colorectal polyps by convolutional neural network features learnt from white light and narrow band endoscopic images of multiple databases. *Annu Int Conf IEEE Eng Med Biol Soc*. 2018;2018:4142-5. https://doi.org/10.1109/EMBC.2018.8513337
8. Saha M, Chakraborty C, Arun I, Ahmed R, Chatterjee S. An advanced deep learning approach for Ki-67 stained hotspot detection and proliferation rate scoring for prognostic evaluation of breast cancer. *Sci Rep*. 2017;7:3213. https://doi.org/10.1038/s41598-017-03405-5
9. Varela G, Jiménez MF, Novoa N, Aranda JL. Estimating hospital costs attributable to prolonged air leak in pulmonary lobectomy. *Eur J Cardiothorac Surg*. 2005;27:329-33. https://doi.org/10.1016/j.ejcts.2004.11.005
10. Brunelli A, Salati M, Pompili C, Gentili P, Sabbatini A. Intraoperative air leak measured after lobectomy is associated with postoperative duration of air leak. *Eur J Cardiothorac Surg*. 2017;52:963-8. https://doi.org/10.1093/ejcts/ezx105
11. Kudo SE, Mori Y, Misawa M, Takeda K, Kudo T, Itoh H, et al. Artificial intelligence and colonoscopy: current status and future perspectives. *Dig Endosc*. 2019;31:363-71. https://doi.org/10.1111/den.13340
12. Toloza EM, Harpole DH Jr. Intraoperative techniques to prevent air leaks. *Chest Surg Clin N Am*. 2002;12:489-505. https://doi.org/10.1016/s1052-3359(02)00020-0
13. Chen-Yoshikawa TF, Fukui T, Nakamura S, Ito T, Kadomatsu Y, Tsubouchi H, et al. Current trends in thoracic surgery. *Nagoya J Med Sci*. 2020;82:161-74. https://doi.org/10.18999/nagjms.82.2.161
14. Domaratzki M, Kidane B. Deus ex machina? Demystifying rather than deifying machine learning. *J Thorac Cardiovasc Surg*. 2022;5:1131-7. https://doi.org/10.1016/j.jtcvs.2021.02.095
15. Liu Y, Chen PC, Krause J, Peng L. How to read articles that use machine learning: users' guides to the medical literature. *JAMA*. 2019;11:1806-16. https://doi.org/10.1001/jama.2019.16489
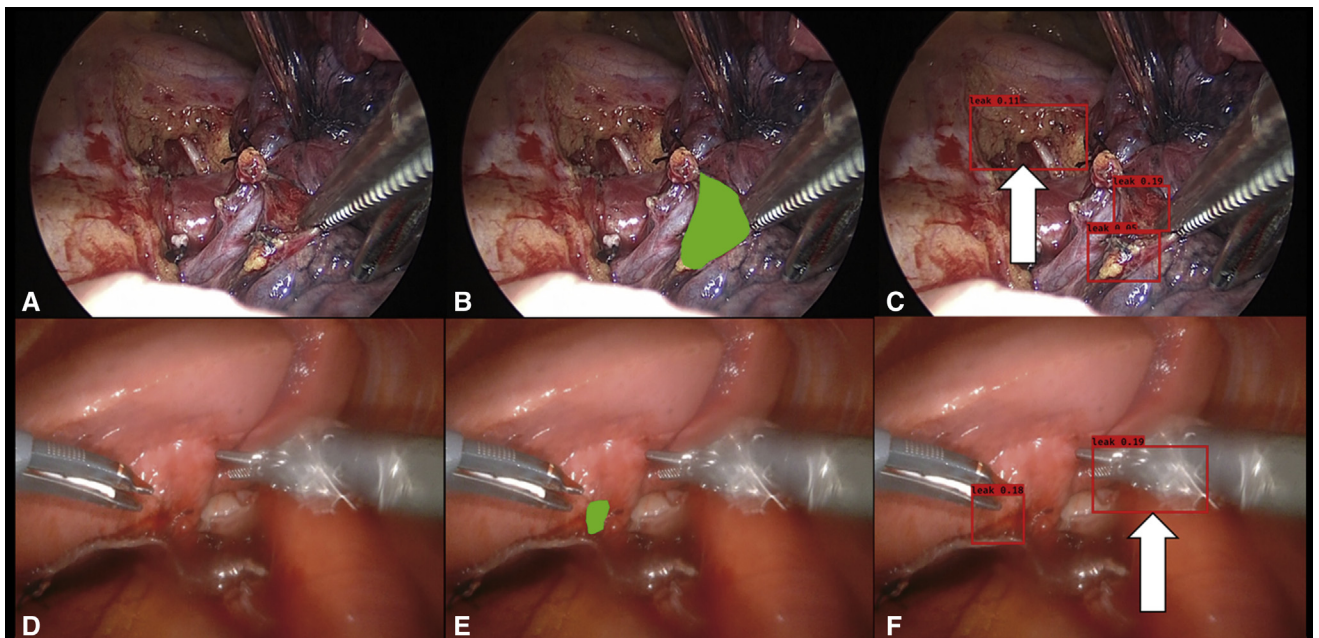
FIGURE E1. False detection of leak sites. A and D, The captured original image. B and E, The actual leak site detected using the conventional leak test. C and F, The output images from the application. *White arrows* indicate incorrectly detected mediastinal fat and surgical instruments.
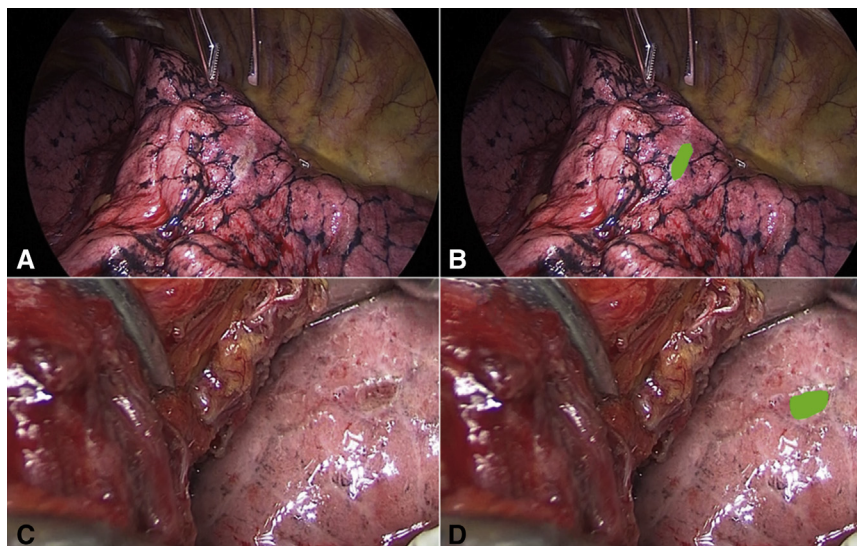
FIGURE E2. Sample cases of false-negative results. A and C, The captured original image. B and D, The actual leak site detected using the traditional leak test. There is only a slight color difference between the background tissue and leak site.

TABLE E1. Clinical data of the leak-positive and leak-negative cases used in the testing phase of this study

Case	Sex	Approach	Surgery	Sites	True leak sites	Confidence score	Category	Procedure to leak site	Postoperative duration of chest tube drainage, d
Leak-positive cases									
1	M	Thoracotomy	Right middle lobectomy	1	Present	0.42	TP	Suture and absorbable mesh covering	2
1				2	Absent	0.08	FP		2
2	M	RATS	Right upper lobectomy	3	Present	0.15	TP	Absorbable mesh covering	5
3	F	RATS	Right lower lobectomy	4	Present	0.52	TP	Absorbable mesh covering	5
3				5	Present	0.2	TP	Absorbable mesh covering	5
4	F	VATS	Right middle lobectomy	6	Present	0.09	TP	Suture	2
5	F	VATS	Right S6 segmentectomy	7	Present	0.51	TP	Absorbable mesh covering	2
6	F	VATS	Left S6 segmentectomy	8	Present	0	FN	Suture and absorbable mesh covering	2
7	F	RATS	Right upper lobectomy	9	Present	0.7	TP	Suture	2
8	M	RATS	Right upper lobectomy	10	Present	0.22	TP	Suture	5
9	F	VATS	Right middle lobectomy	11	Present	0.05	TP	Suture and absorbable mesh covering	2
10	F	RATS	Left upper lobectomy	12	Present	0.08	TP	Suture and absorbable mesh covering	2
11	M	RATS	Left lower lobectomy	13	Present	0.44	TP	Suture and absorbable mesh covering	3
12	M	RATS	Right upper lobectomy	14	Present	0.57	TP	Suture and absorbable mesh covering	2
13	M	VATS	Right upper lobectomy	15	Present	0.07	TP	No additional procedure	2
14	M	VATS	Right upper lobectomy	16	Present	0.11	TP	Fibrin sealant	2
15	M	VATS	Left upper wedge resection	17	Present	0	FN	Suture	5
16	M	Thoracotomy	Right upper lobectomy	18	Present	0.24	TP	Suture and absorbable mesh covering	3
17	F	VATS	Left upper wedge resection	19	Present	0.05	TP	Suture and absorbable mesh covering	4
18	F	RATS	Left lower lobectomy	20	Present	0.46	TP	Absorbable mesh covering	5
19	F	VATS	Right upper lobectomy	21	Present	0	FN	Suture	2
20	F	VATS	Left lower wedge resection	22	Present	0	FN	Suture and absorbable mesh covering	4
21	M	VATS	Right upper lobectomy	23	Present	0.07	TP	Suture and absorbable mesh covering	3
21	M	VATS	Right upper lobectomy	24	Present	0.18	TP	Suture and absorbable mesh covering	3
22	M	VATS	Right lower lobectomy	25	Present	0.23	TP	Suture and absorbable mesh covering	2
23	M	VATS	Left S1+2 segmentectomy	26	Present	0.21	TP	Suture and absorbable mesh covering	4
23				27	Present	0	FN	Suture and absorbable mesh covering	4
23				28	Absent	0.07	FP		4
24	F	RATS	Right lower lobectomy	29	Present	0.45	TP	No additional procedure	4
25	F	Thoracotomy	Right upper lobectomy	30	Present	0	FN	Suture and absorbable mesh covering	7
26	M	VATS	Left upper lobectomy	31	Present	0.13	TP	Suture and absorbable mesh covering	9
27	F	VATS	Left S1 and 2 segmentectomy	32	Present	0.07	TP	Suture and absorbable mesh covering	2

(Continued)

TABLE E1. Continued

Case	Sex	Approach	Surgery	Sites	True leak sites	Confidence score	Category	Procedure to leak site	Postoperative duration of chest tube drainage, d
27				33	Absent	0.07	FP		2
28	M	VATS	Left S8 to S10 segmentectomy	34	Present	0.12	TP	Absorbable mesh covering	2
28				35	Present	0	FN	Absorbable mesh covering	2
29	F	VATS	Left upper lobectomy	36	Present	0.21	TP	Suture and absorbable mesh covering	2
30	F	RATS	Right lower lobectomy	37	Present	0.48	TP	Absorbable mesh covering and Fibrin sealant	2
31	M	VATS	Left upper lobectomy	38	Present	0.09	TP	Suture and absorbable mesh covering	2
32	M	RATS	Right upper lobectomy	39	Present	0.09	TP	Absorbable mesh covering	13
33	M	VATS	Left upper wedge resection	40	Present	0	FN	Suture	1
34	F	VATS	Right S7 to S10 segmentectomy	41	Present	0.06	TP	Suture and absorbable mesh covering	3
35	M	Thoracotomy	Right middle lobectomy	42	Present	0.08	TP	Suture and absorbable mesh covering	2
35				43	Absent	0.13	FP		2
36	M	RATS	Left S6 segmentectomy	44	Present	0.06	TP	Suture and absorbable mesh covering	3
37	F	VATS	Right middle lobectomy	45	Present	0.2	TP	Suture and absorbable mesh covering	2
37				46	Present	0.18	TP	Suture and absorbable mesh covering	2
38	M	Thoracotomy	Right middle lobectomy	47	Present	0	FN	Suture and absorbable mesh covering	2
39	F	VATS	Right lower lobectomy	48	Present	0.57	TP	Suture and absorbable mesh covering	3
39				49	Absent	0.06	FP		3
40	F	RATS	Right S6 segmentectomy	50	Present	0.08	TP	Absorbable mesh covering	6
41	M	Thoracotomy	Left upper wedge resection	51	Present	0.19	TP	Absorbable mesh covering	4
41				52	Present	0.05	TP	Absorbable mesh covering	4
41				53	Absent	0.11	FP		4
42	F	RATS	Right middle lobectomy	54	Present	0.1	TP	Absorbable mesh covering	4
43	F	VATS	Right S7 to S10 segmentectomy	55	Present	0	FN	Suture and absorbable mesh covering	2
44	M	VATS	Left lower wedge resection	56	Present	0	FN	Suture and absorbable mesh covering	2
45	F	RATS	Left lower lobectomy	57	Present	0.1	TP	Absorbable mesh covering	3
45				58	Absent	0.19	FP		3
46	M	VATS	Right upper lobectomy	59	Present	0.05	TP	Absorbable mesh covering	2
47	F	RATS	Right lower lobectomy	60	Present	0.35	TP	Absorbable mesh covering	2
47				61	Absent	0.62	FP		2
48	M	VATS	Left upper segmentectomy	62	Present	0.16	TP	Suture and absorbable mesh covering	3
49	M	VATS	Left upper wedge resection	63	Present	0.47	TP	Resection	2
50	M	VATS	Left upper wedge resection	64	Absent	0	FN	Suture and absorbable mesh covering	3
51	M	RATS	Left lingular segmentectomy	65	Present	0.78	TP	Suture and absorbable mesh covering	3
52	F	VATS	Right upper lobectomy	66	Present	0.1	TP	Suture and absorbable mesh covering	4
53	M	RATS	Left lower lobectomy	67	Present	0.31	TP	Suture	11
54	F	VATS	Right S2 segmentectomy	68	Present	0.16	TP	Fibrin sealant	2

(Continued)

TABLE E1. Continued

Case	Sex	Approach	Surgery	Sites	True leak sites	Confidence score	Category	Procedure to leak site	Postoperative duration of chest tube drainage, d
55	M	VATS	Right Middle and Lower Lobectomy	69	Present	0.25	TP	Absorbable mesh covering	3
56	M	Thoracotomy	Right upper lobectomy	70	Present	0.11	TP	Suture	4
57	M	RATS	Left upper lobectomy	71	Present	0.72	TP	Absorbable mesh covering	8
57				72	Absent	0.06	FP		8
58	F	Thoracotomy	Right upper and middle lobectomy	73	Present	0.11	TP	Suture	3
58				74	Absent	0.08	FP		3
Leak-negative cases									
1	M	RATS	Left upper lobectomy	1	Absent	0	TN		
2	M	RATS	Right upper lobectomy	2	Absent	0	TN		
3	F	VATS	Right S7 to S10 segmentectomy	3	Absent	0	TN		
4	M	VATS	Left upper wedge resection	4	Absent	0	TN		
5	M	Thoracotomy	Left lower lobectomy	5	Absent	0	TN		
6	F	VATS	Left upper wedge resection	6	Absent	0	TN		
7	M	RATS	Right upper lobectomy	7	Absent	0	TN		
8	F	RATS	Right middle lobectomy	8	Absent	0	TN		
9	M	Thoracotomy	Left upper lobectomy	9	Absent	0	TN		
10	M	RATS	Right lower lobectomy	10	Absent	0	TN		
11	M	VATS	Left upper lobectomy	11	Absent	0	TN		
12	M	RATS	Left upper lobectomy	12	Absent	0	TN		
13	F	VATS	Right S6 segmentectomy	13	Absent	0.53	FP		
14	M	VATS	Right upper lobectomy	14	Absent	0.21	FP		
15	M	VATS	Left lower lobectomy	15	Absent	0.1	FP		
16	F	VATS	Left S6 segmentectomy	16	Absent	0	TN		
17	M	RATS	Right lower lobectomy	17	Absent	0	TN		
18	M	RATS	Right upper lobectomy	18	Absent	0	TN		
19	F	VATS	Left upper wedge resection	19	Absent	0	TN		
20	F	VATS	Right upper lobectomy	20	Absent	0.1	FP		
21	M	RATS	Left upper lobectomy	21	Absent	0	TN		
22	M	RATS	Right lower lobectomy	22	Absent	0	TN		
23	F	VATS	Right upper lobectomy	23	Absent	0	TN		
24	M	RATS	Left upper lobectomy	24	Absent	0	TN		
25	F	RATS	Right lower lobectomy	25	Absent	0	TN		
26	M	RATS	Left S8 segmentectomy	26	Absent	0	TN		
27	M	RATS	Right lower lobectomy	27	Absent	0	TN		
28	F	VATS	Right upper lobectomy	28	Absent	0	TN		
29	M	RATS	Right upper lobectomy	29	Absent	0	TN		
30	F	RATS	Left upper lobectomy	30	Absent	0	TN		
31	M	VATS	Left S6 segmentectomy	31	Absent	0	TN		
32	F	RATS	Right lower lobectomy	32	Absent	0	TN		
33	F	RATS	Left upper lobectomy	33	Absent	0	TN		
34	F	RATS	Left upper lobectomy	34	Absent	0	TN		
35	M	RATS	Left lower lobectomy	35	Absent	0	TN		

M, Male; *TP*, true positive; *FP*, false positive; *F*, female; *VATS*, video-assisted thoracoscopic surgery; *FN*, false negative; *RATS*, robot-assisted thoracic surgery; *TN*, true negative.